

# **Insect Solutions for Open Self-Cleaning Microfluidics**

Chengqi Zhang, Peter H. Adler, and Konstantin G. Kornev\*

Insect feeding devices with unobstructed channels offer a wetting—dewetting dichotomy that allows fluid to be self-contained but the channels to be self-cleaning. An explanation of this unprecedented robustness is previously lacking. C-faced channels are fabricated with different openings and their surfaces are modified to study the effects of different contact angles on channel wettability. X-ray microcomputed tomography (micro-CT) reveals hidden features of wetting—dewetting transitions of droplets in these channels. A wetting—dewetting phase diagram is theoretically constructed and experimentally validated to reveal the conditions for which a liquid will spread to form a column that is self-contained in these channels. This study significantly relaxes the requirements for materials to be wettable and self-contain fluids. This work offers promising new applications for microfluidics that can keep the empty channels clean but allow efficient transport of probing liquids.

#### 1. Introduction

Insects have developed unique mechanisms for fluid handling, typically with little influence from gravity. These mechanisms allow insects to exploit diverse foods, such as floral nectar, fruit, sap, blood, sweat, and tears.[1] Over evolutionary time, insect fluidic systems reached unprecedented robustness, with unobstructed channels affording a wetting-dewetting dichotomy that allows fluid to be self-contained but the channels to be self-cleaning. An explanation for the wetting-dewetting dichotomy and robustness of open channels is lacking. The problem concerns not only biologists. Microfluidic devices with open channels have unique technical advantages compared with closed-channel microfluidics that prompted the development of lab-on-a-chip technologies to fabricate these devices.<sup>[2]</sup> In open linear channels with relatively simple geometry, liquid specimens can take on different equilibrium configurations, forming droplets, extended columns, and wedges.[3] The wetting-dewetting transition is manifested through the transition from an extended liquid column that spreads over the channel but remains in the channel, to a clamshell-like droplet that

Dr. C. Zhang, Prof. K. G. Kornev
Department of Materials Science & Engineering
Clemson University
Clemson, SC 29634, USA
E-mail: kkornev@clemson.edu
Prof. P. H. Adler
Department of Plant and Environmental Sciences
Clemson University
Clemson, SC 29634, USA

The ORCID identification number(s) for the author(s) of this article can be found under https://doi.org/10.1002/admi.201901516.

DOI: 10.1002/admi.201901516

bulges above the channel edges and is easily shaken off. Design of open channels is demanding because the shape of the free liquid surface has to be predicted and controlled to guarantee that the liquid will be confined to the channel. Thus, channel openness and its shape represent a package; one implies the other.

Engineering designs of microchannels are mostly limited to those with sharp corners, such as rectangular and V-shaped channels. These designs significantly narrow the range of materials appropriate for microfluidic applications. For example, to keep liquid inside open rectangular channels, the capillary Laplace pressure must be below atmospheric; the wetting-dewetting phase diagram con-

structed for rectangular grooves<sup>[4,2a]</sup> demands that the channel materials form low contact angles with the liquids in question. These requirements exclude the most popular and inexpensive thermoplastics, such as polyethylene, polypropylene, and polystyrene, as possible candidates for analysis of aqueous biofluids and blood. To use these materials, one has to functionalize the channel surface for open microfluidic applications.

A search for an alternative design of open fluidic channels has been initiated in response to progress in development of fiber-spinning technology; this technology offers new opportunities to directly melt extrude inexpensive open channel microfluidics.<sup>[5]</sup> Fibers with different cross-sectional shapes can be spun from inexpensive thermoplastics and used as fiber-based microfluidic devices. Due to hydrodynamic instability during fiber spinning, the channels on fiber surfaces have a common ground plan: they are C-faced with round edges.

Conduits with C-faces are abundant in the living world, particularly among arthropods (Figure 1). The ability of multifunctional chitinous cuticle<sup>[6]</sup> to provide rigid boundaries for flow predisposes arthropods to the expression of channels. Coupled with various surface textures and chemistries, such as lipid-rich coatings, cuticle can provide channels with versatile wettability functions.<sup>[7]</sup> Although most natural C-faced cuticular channels are closed,<sup>[8]</sup> open C-channels are well represented in feeding devices of insects.<sup>[9]</sup>

Inspired by microfluidic devices of insects, we considered C-faced channels as candidates for fiber-based microfluidics. The contact angle that water makes with the cuticular walls of natural microfluidic channels varies over a broad range. [10] We, therefore, asked whether an open C-channel can relax the requirements on the contact angle to broaden the library of materials that can contain liquid columns while simultaneously keeping the channel clean.

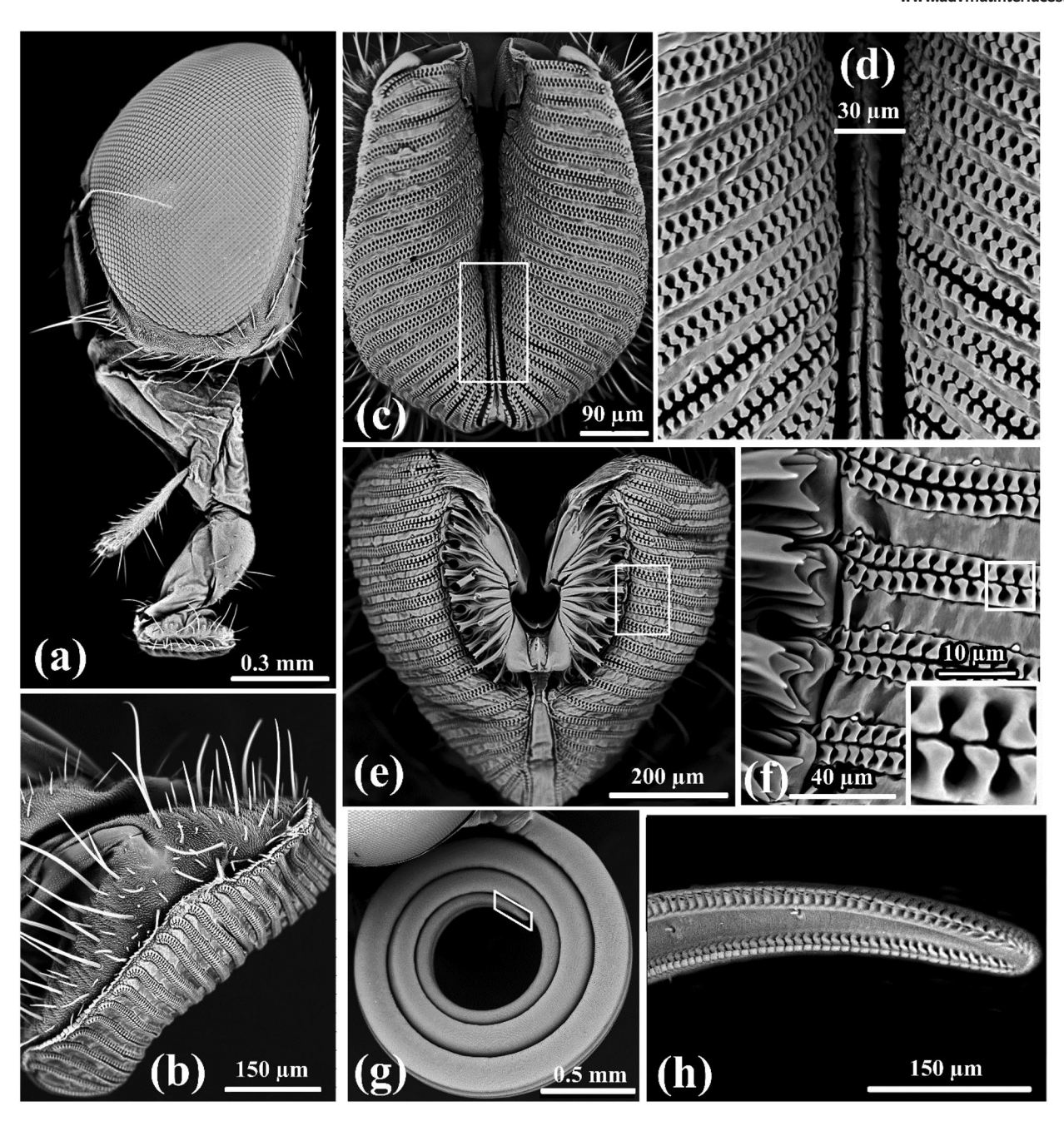


Figure 1. Open C-faced channels in selected mouthparts of insects. a) Head of a fly (Calliphoridae) and its proboscis, lateral view. b) Distalmost portion of the proboscis, lateral view, showing pseudotracheae along the margin. c–f) Fluid-collecting surface of the distal surface of a fly's proboscis, showing pseudotracheae. Fluid enters the rounded openings of the first level of channels. c,e) Entire distal proboscis surface of two species; white boxes indicate areas enlarged in (d) and (f), with boxed area of (f) indicating further enlargement (inset). g,h) Proboscis of monarch butterfly (Danaus plexippus), g) coiled; boxed area indicates the exposed, open food channel at the tip of one half (galea) of the proboscis in (h).

### 2. Results and Discussion

Five C-faced channels were fabricated from polydimethylsi-loxane (PDMS), with different opening angles,  $2\beta = 158^{\circ}$ ,  $170^{\circ}$ ,  $190^{\circ}$ ,  $220^{\circ}$ ,  $240^{\circ}$ , using a molding technique (**Figure 2**a–c; details in the Experimental Section). Different silanes were applied from the vapor phase to change the surface energy of the channels, giving different contact angles with the wetting

liquids. However, the silane coatings are not able to achieve high surface energy. Thus, we coated the channels with platinum (Experimental Section). We also used different wetting liquids (iohexol, glycerin, and mercury) to produce a wide range of contact angle data (Table 1). Iohexol and glycerin have contact angles of nearly 0° with the platinum-coated channels, and mercury has contact angles similar to those with the silane-coated channels. For these cases, instead of repeating the

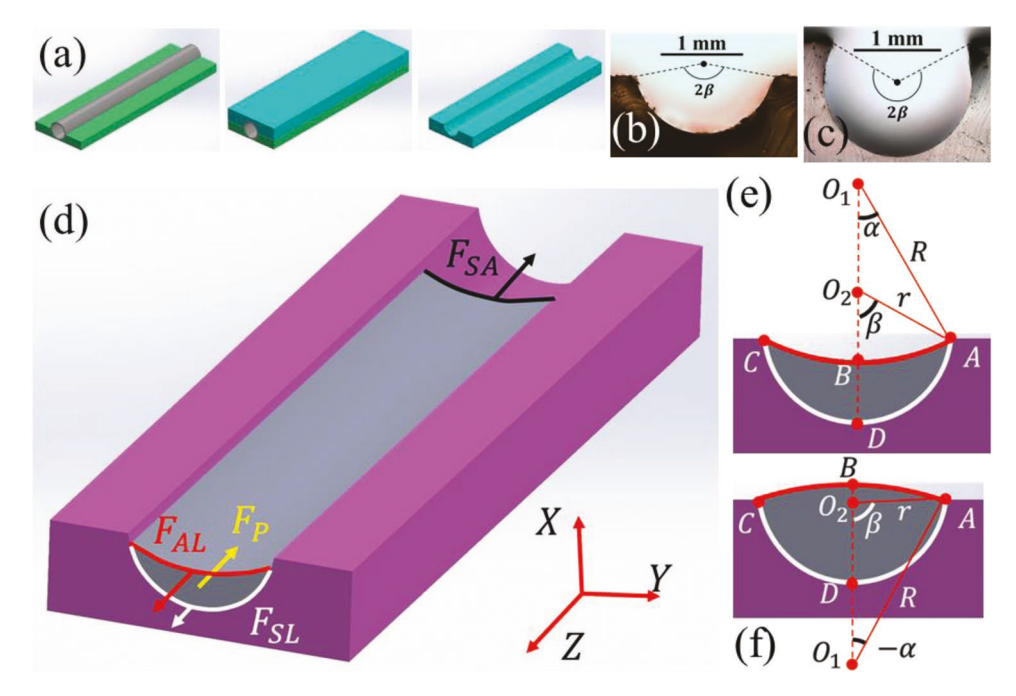


Figure 2. PDMS C-faced channels and different configurations of menisci of the liquid columns inside these channels. a) The three steps of the channel fabrication process, showing the wax mold (green) with embedded tube; this mold was covered with a PDMS layer and the wax and the tube were removed after curing of PDMS. b,c) Cross-sections of fabricated PDMS C-faced channels with opening angle  $2\beta = 158^{\circ}$  and  $2\beta = 240^{\circ}$ , respectively. d) Liquid column inside the C-faced channel: schematic for analysis of the free body diagram. e) Liquid column with concave meniscus; the column cross-section shows two contact lines (solid dots C and A) pinned at the channel edges. f) Liquid column with convex meniscus, showing two contact lines (solid dots C and A) pinned at the channel edges.

experiments for the same contact angle, we selected "IP" and "MH" in Table 1 as representatives.

The configurations of liquid bodies in C-faced channels were studied with the Bruker Skyscan 1176 X-Ray Micro-CT scanner with 9  $\mu$ m resolution. The procedures are described in the Experimental Section. A series of 3D images of liquid bodies and their 2D cross-sections are shown in **Figure 3**a–f. Our results for wetting of the lepidopteran galea<sup>[10b]</sup> show that droplets take on similar shapes (Figure 3g–m).

Analysis of configurations of liquid bodies of all studied liquids allows us to suggest that all equilibrium shapes of the observed liquid bodies can be categorized as clamshell (Figure 3a) and column (Figure 3c,e,g,j,l). The radius of the cross-sectional meniscus for the columns remains almost constant except at the ends where it gradually decreases (Figure 3n). Therefore, the columns are distinguished from the clamshells

by having one of their two principal curvatures go to zero, i.e.,  $d^2R/dz^2=0$  (Video S1 in the Supporting Information is the "MH" pair with channel opening angle  $2\beta=220^\circ$ ; Video S2 in the Supporting Information is the "MH" pair with  $2\beta=190^\circ$ ; Video S3 in the Supporting Information is the "MP" pair with  $2\beta=240^\circ$ ; Video S4 in the Supporting Information is the "MP" pair with  $2\beta=220^\circ$ ).

It is surprising and counterintuitive that the C-channels with re-entrant geometry of their edges and large contact angles allow liquid columns to spread over the channels but do not allow fluid to overflow the edges and spread over the planar substrate (Figure 3e,f,(ii,iii)). One would expect that the convex menisci in the columns generating positive capillary pressure greater than the atmospheric pressure would push the liquid out of the channel. Yet, the columns remain self-contained in the channels and the contact lines pinned to the channel edges.

Table 1. Contact angle between wetting liquids and C-faced channels. Each pair of a channel surface and a wetting liquid is coded with a two-letter format (e.g., IG).

| Channel Surface  | Wetting Liquid          |                         |                          |
|--|-------------------------|-------------------------|--------------------------|
|  | Iohexol                 | Glycerin                | Mercury                  |
| (3-glycidyloxypropyl) trimethoxysilane                     | $23 \pm 5^{\circ} (IG)$ | 45 ± 3°(GG)             | 135 ± 3°(MG)             |
| 3-methacryloxypropyl trimethoxysilane                      | $38\pm4^{\circ}(IM)$    | $74 \pm 5^{\circ} (GM)$ | $136 \pm 4^{\circ} (MM)$ |
| Trimethylethoxysilane                                      | $48 \pm 4^{\circ}$ (IT) | 88 ± 4°(GT)             | $137 \pm 3^{\circ} (MT)$ |
| n-octyldimethyl chlorosilane                               | $68 \pm 5^{\circ} (IO)$ | 93 ± 5°(GO)             | 139 ± 3° (MO)            |
| (heptadecafluoro-1 1 2 2-tetrahydrodecyl) trimethoxysilane | $84 \pm 4^{\circ} (IH)$ | 106 ± 4° (GH)           | 138 ± 3° (MH)            |
| Platinum   | 6°± 3 (IP)              | 7°± 4(GP)               | $101 \pm 7^{\circ} (MP)$ |

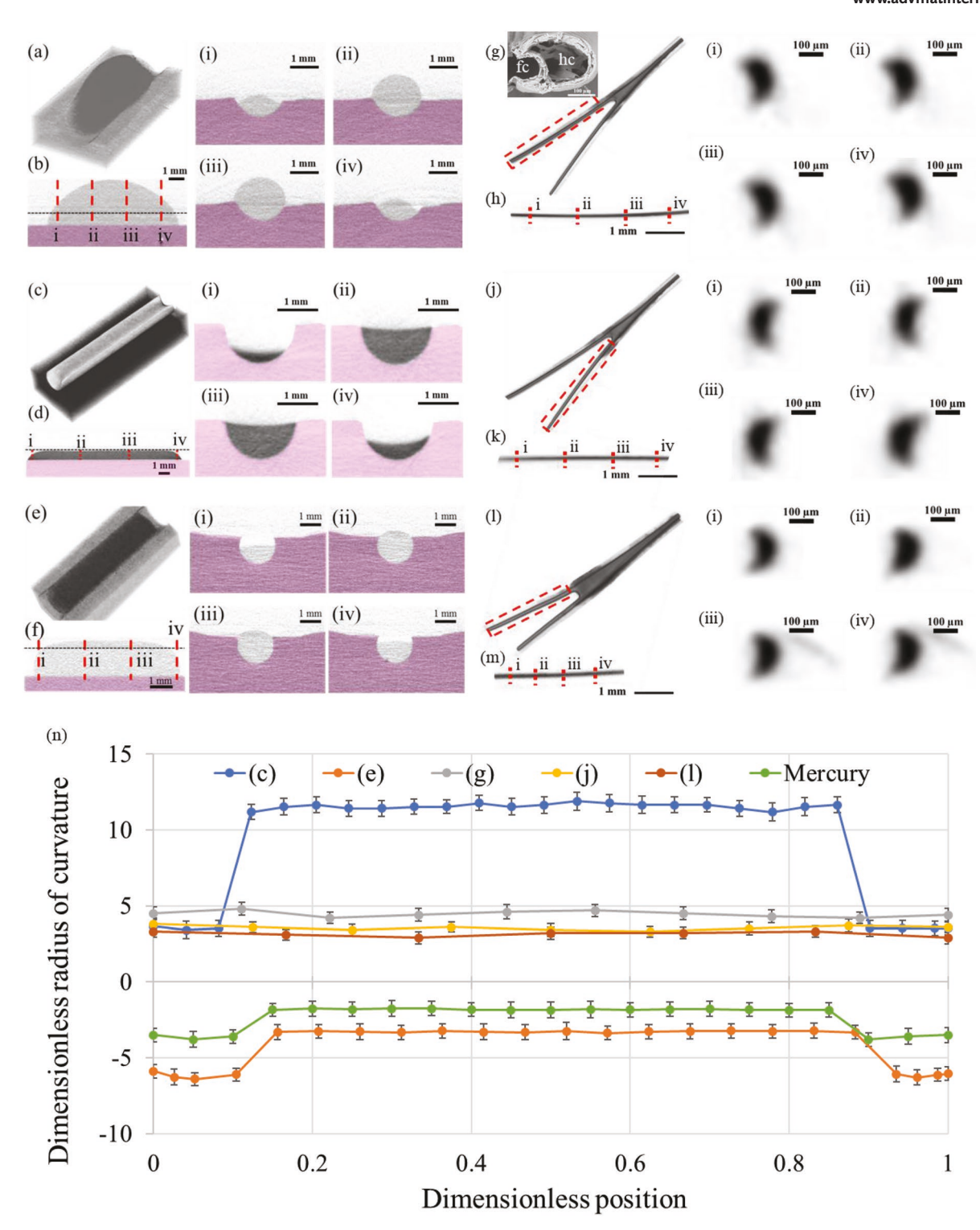


Figure 3. 3D configurations of liquid bodies and their 2D cross-sections in C-faced channels. To distinguish the original gray image of the drop, the PDMS substrate is colored in pink. Dashed lines specify the channel edges. a-m) Cross-sections at positions (i), (ii), (iii), and (iv) are shown in separate images (i), (ii), (iii), and (iv) on the right. a) Clamshell glycerin droplet in a C-faced channel with opening angle  $2\beta = 158^{\circ}$  and contact angle  $\theta = 88^{\circ}$ . b) Side view of the clamshell. c) Iohexol column in a C-faced channel with opening angle  $2\beta = 170^{\circ}$  and contact angle  $\theta = 38^{\circ}$ . d) Side view of the liquid column. e) Glycerin column in a C-faced channel with opening angle  $2\beta = 220^{\circ}$  and contact angle  $\theta = 93^{\circ}$ . f) Side view of liquid column. g,j,l) Iohexol columns in half of the lepidopteran food canal of one galea, with opening angle  $2\beta = 180^{\circ}$  and contact angle  $\theta = 0^{\circ}$ . h,k,m) Side view of the liquid column in the lepidopteran food canal. n) Dependence of dimensionless radius R (normalized by the channel radius) of the meniscus in cross-sections of the liquid columns in (c), (e), (g), (j), (l) and a column formed by liquid mercury on the dimensionless positions along the channel. The radius is considered positive when menisci are concave, as in (d), (h), (j), and (l), and it is considered negative when menisci are convex, as in (f).

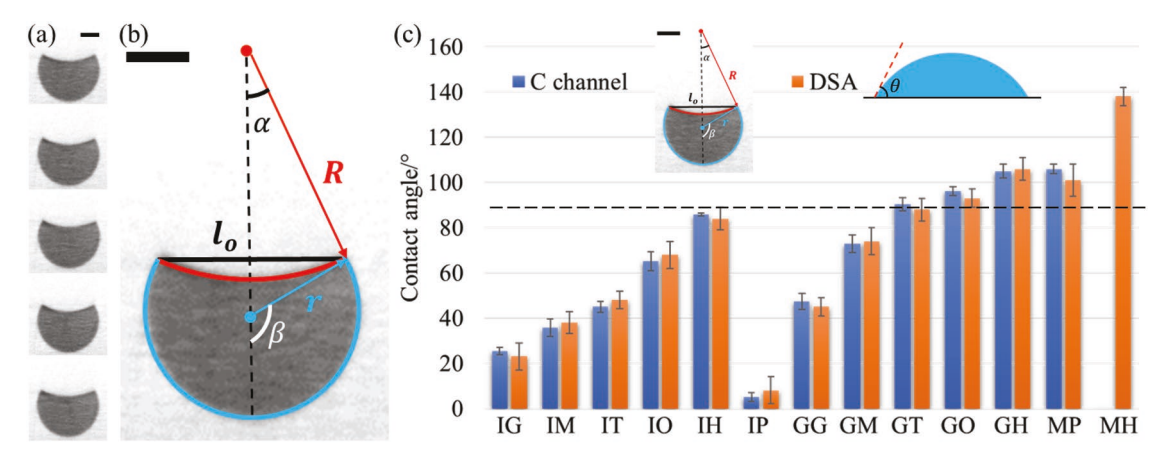


Figure 4. a) Measurements of the contact angles of liquid columns. Five cross-sections taken at the middle of the liquid column allow the necessary parameters to be extracted for the contact angle measurement as shown in (b). Scale bars = 0.5 mm. c) Comparison of indirect measurements of contact angles from X-ray images with those from Kruss DSA 10 in Table 1. The dashed line corresponds to a contact angle of 90°. Because liquid mercury could not form a column in (heptadecafluoro-1 1 2 2-tetrahydrodecyl)trimethoxysilane coated PDMS C-faced channels, there is no "C channel" measurement for "MH."

To explain this behavior, we turned to the Laplace law of capillarity and analyzed equilibrium shapes of the liquid columns to determine the conditions when this columnar solution disappears.

In experiments, the channel radius was r = 0.85 mm, which is much smaller than the capillary length,  $l_c = \sqrt{\sigma / \rho g}$ , where  $\sigma$  is the surface tension,  $\rho$  is the liquid density, g is the acceleration due to gravity. For glycerin  $l_c = 2.26$  mm, for iohexol  $l_c = 2.31$  mm, for mercury  $l_c = 60.43$  mm. Thus, the inequality  $r/l_c < 1$  holds true and gravity can be neglected, suggesting that the pressure inside the liquid columns should be almost constant. The channel and liquid drops are macroscopic; therefore, in the boundary conditions for the Laplace equation, the line tension can be neglected. The Laplace equation of capillarity is written in the form  $\sigma \nabla n = P$ , where vector n is the outward unit normal vector to the air/liquid interface, the dot product is the mean curvature of the air/liquid interface, and P is the pressure in the drop measured relative to atmospheric pressure. The column wets the channel; that is, the contact lines at the ends of the column must be sitting inside the channel. The Laplace equation of capillarity has the first integral stating the force balance in the axial channel direction. [10b,11] The clamshell to column transition is explained by the analysis of this force balance equation.

Introducing the Cartesian system of coordinates (x, y, z), where the channel is parallel to the z-axis (Figure 2d), the free body diagram for the column is built up by making an imaginary cut perpendicular to the channel axis z in the middle of the column (Figure 2d). One half of the column is then replaced with an equivalent system of forces acting in the z-direction parallel to the channel long axis

$$F_{AL} + F_{SL} - F_{SA} - F_{P} = 0 ag{1}$$

where  $F_{AL}$  is the force due to surface tension  $\sigma_{AL}$  at the air/liquid interface;  $F_{SL}$  is the force due to surface tension  $\sigma_{SL}$  at the solid/liquid interface;  $F_{SA}$  is the force due to surface tension  $\sigma_{SA}$  of the

solid/air interface;  $F_P$  is the resultant pressure acting perpendicular to the cross-section of area in the z-direction. Equation (1) is analyzed in detail in the Supporting Information where we prove that the equilibrium liquid columns can exist if and only if the contact lines remain pinned at the channel edges. This fact was confirmed experimentally: the contact lines of all equilibrium columns remained pinned at the channel edges. The Videos S3 and S4 in the Supporting Information of the mercury/platinum pair illustrates this statement; this pair provides the best micro-CT contrast, allowing the sharp edges of the channel to be distinguished where the contact line of the column is pinned.

The contact angle on the flat part of the PDMS chips was measured with Kruss Drop Shape Analyzer (DSA 10) (Table 1). To compare these contact angles with those formed at the contact lines inside the channels at the column ends, we used X-ray images from which the channel radius r, meniscus radius R, and opening width  $l_0$  were measured. The effect of the contact line pinning at the channel edges is also clearly seen in **Figure 4**a,b. As shown in the Supporting Information, the contact angle depends on these parameters as

$$\theta = \arccos \left\{ \left[ \alpha \left( \sin \beta / \sin \alpha \right) + \beta \left( \sin \alpha / \sin \beta \right) + \sin \left( \beta - \alpha \right) \right] / 2\beta \right\},$$

$$\alpha = \arcsin \left( l_0 / 2R \right), \beta = \arcsin \left( l_0 / 2r \right)$$
(2)

Substituting the measured parameters into these formulas and calculating the contact angles, we confirmed that the results obtained with these two methods are close to each other, proving that the developed theory can be further applied to construct the wetting–dewetting phase diagram for these channels (Figure 4).

As explained in the Supporting Information, the wetting—dewetting transition can be associated with the disappearance of columnar solutions satisfying Equation (1). When liquid columns cannot be formed in the C-faced channels, the liquid will be gathered into clamshell droplets. The criterion for disappearance of the columnar solutions is  $\alpha = -90^{\circ}$ . Substituting this  $\alpha$  in the first Equation (2), we obtain

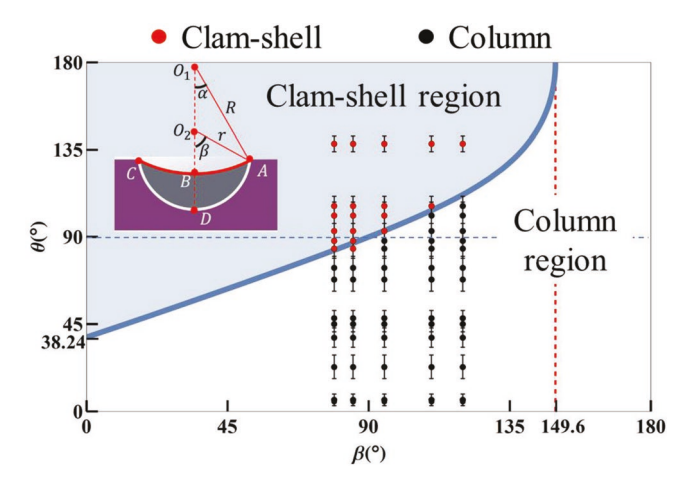


**Figure 5.** The wetting–dewetting phase diagram for C-faced channels in terms of contact angle  $\theta$  and channel opening angle  $\beta$ . The shaded region above the solid line describes nonwettable channels where liquid will gather in clamshells; clamshells exist only in channels with opening angle  $\beta$  < 149.6° marked by the red dashed line. The solid line describes wettable channels where liquid will form a self-contained column. The black solid dots are experimentally observed columns and the red solid dots are experimentally observed clamshells.

$$\theta = \arccos\left[\left(\frac{\pi}{2}\sin^2\beta - \beta + \cos\beta\sin\beta\right)/(2\beta\sin\beta)\right]$$
 (3)

In the  $\theta$ – $\beta$  plane, Equation (3) separates the region of contact angles  $\theta$  and the channel opening angles  $\beta$  where the liquid columns can exist from the region where only clamshells can be found (**Figure 5**). A singularity exists when the C-faced channel turns into a flat ribbon,  $\beta \to 0$ . The contact angle in this scenario is obtained from Equation (3) as  $\theta$  = arc cos ( $\pi$ /4) = 38.24°, which agrees with the prediction for the ribbon and stripe. [11] The experimental results were placed in Figure 5 and compared with theoretical predictions, demonstrating a good match. This suggests that the constructed phase diagram fully describes the behavior of liquids in the C-faced channels.

The exciting result from Figure 4 is that the columns can be obtained within the C-channels of nonwettable materials even when the drop makes contact angles greater than 90° with a flat surface of the same material. In this case, the dry channel remains clean when the droplets are placed atop the channel. We illustrate this behavior using a glycerin droplet that makes a 106° contact angle with a silanized PDMS chip (Figure 6). The droplet neither wetted nor invaded the channel even after more liquid was added. The meniscus pinned at the channel edges

remained almost unperturbed while the drop spread over the flat side of the chip under its own weight.

Feeding devices of insects provide diverse examples of channel modifications for engineered microfluidics (Figure 1). The manufactured C-faced channels shown in Figure 2 can be considered as good models of pseudotracheal channels of flies, having somewhat similar cross-sections shown in the insert of Figure 1f and of C-faced channel of lepidopteran galeae shown in Figure 1h. Pseudotracheal channels are smooth like those of the PDMS models. The C-faced channels of lepidopteran galeae are ribbed with a rib diameter of tens of micrometers for Manduca sexta and smaller for finer proboscises. The features of these surface sculpturings are much smaller than the channel diameter; hence one can treat this sculptured surface as a smooth surface with an overlaid certain roughness. In our PDMS models, the surfaces are smooth but we have changed the contact angle to effectively take into account this effect of the surface roughness.

Larval diving beetles (Dytiscidae) have suctorial mandibles, each with an open (or closed) C-faced channel through which digestive enzymes are pumped into prey and the liquefied food ingested.[12] Absence of mandibular channels is the ancestral condition, but open channels appeared early in the family's evolutionary history, and subsequent evolution produced open and closed channels multiple times.[13] In Lepidoptera, the evolutionary trend was toward channel closure, with increasingly tight linkage to accommodate insertion of the proboscis into floral tubes.[9b] Yet, open channels were retained in the oldest extant Lepidoptera with a proboscis, and reversions to open channels, typically in concert with proboscis shortening,[14] occurred deep within the lineage of closed-channel Lepidoptera, providing new modes of fluid uptake. [15] If the two halves of the proboscis become separated (Figure 1h), the open channels can continue transporting liquid [10b,16] (Video S5 in the Supporting Information shows water uptake by a single separated galea of Monarch proboscis). The astounding diversity of flies-more than 150 000 species-presents rich diversity in the hierarchical, cuticular network of open C-channels (pseudotracheae) at the end of the proboscis (Figure 1a–f). Open pseudotracheal channels, which bring fluid to a central food channel, became variously fitted with cuticular brushes and plates over evolutionary time to serve a range of additional functions,<sup>[17]</sup> such as tissue abrasion and debris filtering.<sup>[18]</sup> The terminal portion (haustellum) of the proboscis of some adult caddisflies (Trichoptera) has a cuticular system of channels (13-22 µm diameter) for fluid uptake, with their open faces roofed by fine hairs for filtering liquids.<sup>[19]</sup> The expanded

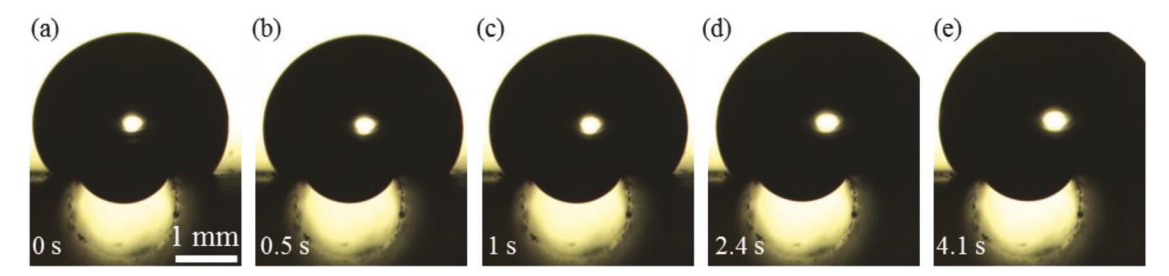


**Figure 6.** Behavior of a glycerin droplet applied from the top to a C-faced channel with an opening angle of 240° and contact angles of 106°. After 1 s, more glycerin was injected into the drop; the drop reacts to the addition of this extra volume by spreading to the right.

www.advancedsciencenews.com



www.advmatinterfaces.de

fluid-collecting surfaces of the fly and caddisfly proboscises provide intriguing opportunities for an optimized number of channels and a mosaic of channel types, varying in the degree of closure, armature, and wettability. The wetting/dewetting phase diagram in Figure 5 offers new metrics for classification of natural open C-faced channels.

## 3. Conclusion

We have demonstrated a design for bioinspired C-channels that can be used to transport fluids in open microfluidics when fluid in a channel is exposed to the atmosphere or to another fluid. We also explained the wetting dichotomy by constructing a wetting-dewetting phase diagram and validating it experimentally. An open C-design allows fluid to cover the surface of the channel while remaining in the trough. Unobstructed channels are essential for optimal function, and C-channels are self-cleaning. The necessity for self-cleaning channels in Nature is seen, for example, in fluid-feeding insects that exploit organically rich substances such as blood and nectar to which debris and biofilms could adhere. We have provided an explanation for the robustness of C-channels, quantitatively specifying the conditions for the channel opening and surface energy of a solid material, when the channel can be protected from entry of debris or liquid droplets within a certain range of surface energy. The proposed design opens a wide range of possible microfluidic applications for using channeled fibers fashioned from inexpensive thermoplastics.

Potential microfluidic designs and applications can be inspired by the abundance of natural templates. Nature has exploited the versatility of cuticle and its properties to form channels with diverse fluid-transport roles. By varying the degree of channel closure and associated cuticular modifications, insects can enhance functionality, such as capillarity, flow, and filtering.<sup>[20]</sup>

Inspired by examples in insect cuticle, we demonstrated the conditions under which open C-faced channels will transport fluid while also remaining clean. Our methodology and developed diagram for the clamshell/column transition of droplets in C-faced channels can be further generalized for analysis of other attractive channel shapes exploited by Nature over millions of years of evolution.

## 4. Experimental Section

Preparation of C-Faced Channels with Various Shapes: C-faced channels with different opening angles were fabricated through reverse polymer molding with PDMS, following the experimental protocol schematically illustrated in Figure 2a.

The reverse molds for fabricating the C-faced channels with different opening angles were constructed by embedding the capillary tube in a wax substrate. A paraffin wax (Carolina Biological Supply Company) was melted at 80 °C in a glass Petri dish, and the capillary tube with a diameter of 1.7 mm was horizontally embedded in the liquid wax. The capillary tube was touching the bottom of the Petri dish, and the molten wax was poured to submerse the tube at different depths. In this way, channels can be made with different opening angles. The wax/capillary mold was then solidified at room temperature for 30 min, and the solid wax menisci, which were formed by liquid wax wetting the walls of the

capillary tube, were removed with a sculpting knife to form a flat surface near the capillary tube region.

SYLGARD 184 Silicone Elastomer Base was mixed with SYLGARD 184 Silicone Elastomer Curing agent with mass ratio 10:1. After fully mixing and removing bubbles in a plastic Petri dish, the mixture was poured on the wax/capillary mold and cured at room temperature for 24 h. After curing, the solidified PDMS layer was detached from the mold and the final C-faced channel was obtained. By this method, five C-faced channels with different opening angles,  $2\beta = 158^{\circ}$ ,  $170^{\circ}$ ,  $190^{\circ}$ ,  $220^{\circ}$ ,  $240^{\circ}$ , were fabricated.

Contact Angle Control through Silanization: To permanently increase the surface energy of the PDMS channel surface, chemical vapor deposition (CVD) of silanes was chosen to conduct the surface modification.

Each channel was cut into four pieces. The cut channels were placed in the plasma instrument at the highest setting (PLASMA CLEANER/ STERILIZER, Harrick Scientific Corp, PDC-32G, Input power 100 W, Highest settings: 720 V DC, 25 mA DC, Applied to 18 W) for 15 min to activate the surface. After the plasma treatment, they were put in three 50 mL VWR Polypropylene Centrifuge Tubes with silanes present, and then left for CVD overnight to graft silanes to the surface. Five types of silanes were used to modify the four pieces of channels of each type to obtain different surface energies: (3-glycidyloxypropyl)trimethoxysilane, 3-methacryloxypropyltrimethoxysilane, trimethylethoxysilane, n-octyldmethylchlorosilane, and (heptadecafluoro-1 1 2 2-tetrahydrodecyl) trimethoxysilane.

After the surface modification, the contact angles between the channels and the wetting liquids, OMNIPAQUE (lohexol) Injection and glycerin (surface tensions: 80 and 64 mN m<sup>-1</sup>, respectively), were measured on a flat surface next to the channel, using Kruss Drop Shape Analyzer (DSA 10) with the "Tangent method 1." Based on the sample preparation process described below in (d), the contact angle between the substrates and the wetting liquids should be equilibrium advancing contact angle. The results are given in Table 1.

Contact Angle Control through Platinum Coating: To obtain more experimental data at the phobic region where the contact angle was greater than 90°, mercury was used as the wetting liquid, and a platinum coated PDMS C-face as the substrate.

For platinum coating, the PDMS channels were placed in a sputter-coating instrument (HummerTM SC6.6, coating pressure 80 Pa, current 15  $\mu$ A) for 1.5 min. The contact angles between the platinum coated channel and mercury (surface tension 486.5 mN m $^{-1}$ ) was measured on a flat surface next to the channel, using Kruss Drop Shape Analyzer (DSA 10) with the "Tangent method 1." The results are in Table 1.

Formation of Liquid Body in C-Faced Channel: The wetting liquids were acquired from the reservoir with a micropipette, and then injected into the C-faced channels. During injection, the tip of the micropipette remained close to the opening of the channel, so that the wetting liquids were directly injected into the channel without touching the surfaces outside. The process was recorded in Video S6 in the Supporting Information; mercury was used as an example. After the injection, the samples were placed on a flat table for five minutes enabling full spreading of the liquid.

Micro-CT Imaging and Analysis Procedures: After the liquid fully spread and acquired the equilibrium configuration, the channel with the liquid body was taped to a semi-cylindrical stage made of a plastic foam transparent to the X-rays. The stage was placed on a semi-cylindrical holder inside the micro-CT scanner so that the flat surface of the PDMS chip was oriented horizontally, ensuring that the C-faced channel was sitting at the center of the holder. The filter, voltage, and current were selected based on the wetting liquid used. No filter, 90 kV voltage, and 276 μA current were used for imaging the iohexol (OMNIPAQUE Injection) and mercury droplets. A 0.2 mm thick aluminum filter, 65 kV voltage, and 383 μA current were set for imaging glycerin droplets. NRecon Reconstruction software was used to reconstruct the 3D configurations; the 3D droplet configurations were viewed with CTVox and the cross-sections were acquired with DATAVIEWER

www.advancedsciencenews.com



www.advmatinterfaces.de

# **Supporting Information**

Supporting Information is available from the Wiley Online Library or from the authors.

# **Acknowledgements**

This work was supported in part by National Science Foundation SC EPSCoR/IDeA Program award no. OIA-1655740. The authors thank Julia Brumaghim for sharing mercury; Christopher Weber, and the Office of Research Safety at Clemson University for helping them to develop the protocol for using mercury; and the Godley-Snell Research Center at Clemson University for letting them use the micro-CT.

### **Conflict of Interest**

The authors declare no conflict of interest.

# **Keywords**

biomimetics, hydrophobic/philic surfaces, microfluidics, surface modification, wetting

Received: September 2, 2019 Revised: September 29, 2019 Published online:

- a) V. B. Wigglesworth, The Life of Insects, Weidenfeld and Nicolson, New York 1972; b) J. G. Kingsolver, T. L. Daniel, Regulatory Mechanisms in Insect Feeding (Eds: R. F. Chapman, G. deBoer), Springer, New York 1995, p. 32.
- [2] a) R. Seemann, M. Brinkmann, E. J. Kramer, F. F. Lange, R. Lipowsky, Proc. Natl. Acad. Sci. USA 2005, 102, 1848;
  b) G. M. Whitesides, E. Ostuni, S. Takayama, X. Jiang, D. E. Ingber, Annu. Rev. Biomed. Eng. 2001, 3, 335;
  c) B. P. Casavant, E. Berthier, A. B. Theberge, J. Berthier, S. I. Montanez-Sauri, L. L. Bischel, K. Brakke, C. J. Hedman, W. Bushman, N. P. Keller, D. J. Beebe, Proc. Natl. Acad. Sci. USA 2013, 110, 10111;
  d) M. Zhang, S. Feng, L. Wang, Y. Zheng, Biotribology 2016, 5, 31;
  e) J. Peng, X. Zhao, W. Wang, X. Gong, Langmuir 2019, 35, 8404;
  f) Q. Borjihan, J. Yang, Q. Song, L. Gao, M. Xu, T. Gao, W. Liu, P. Li, Q. Li, A. Dong, Biomater. Sci. 2019, 7, 3334.
- [3] J. Berthier, K. A. Brakke, E. Berthier, Open Microfluidics, Wiley-Scrivener, Beverly, MA 2016.

- [4] a) R. Seemann, M. Brinkmann, S. Herminghaus, K. Khare, B. M. Law, S. McBride, K. Kostourou, E. Gurevich, S. Bommer, C. Herrmann, D. Michler, J. Phys.: Condens. Matter 2011, 23, 184108; b) V. T. Gurumurthy, I. V. Roisman, C. Tropea, S. Garoff, J. Colloid Interface Sci. 2018, 527, 151.
- [5] a) T. Hongu, G. O. Phillips, M. Takigami, New Millenium Fibers, Woodhead Publishing Ltd, Cambridge 2005; b) A. Yildirim, M. Yunusa, F. E. Ozturk, M. Kanik, M. Bayindir, Adv. Funct. Mater. 2014, 24, 4569; c) M. Yunusa, F. E. Ozturk, A. Yildirim, U. Tuvshindorj, M. Kanik, M. Bayindir, RSC Adv. 2017, 7, 15553; d) D. M. Nelson, R. D. Stanelle, P. Brown, R. K. Marcus, Am. Lab. 2005, 37, 28. e) A. J. Schadock-Hewitt, J. J. Pittman, K. A. Stevens, R. K. Marcus, J. Appl. Polym. Sci. 2013, 128, 1257.
- [6] J. F. V. Vincent, U. G. K. Wegst, Arthropod Struct. Dev. 2004, 33, 187.
- [7] R. Hensel, C. Neinhuis, C. Werner, Chem. Soc. Rev. 2016, 45, 323.
- [8] a) M. H. Rahman, M. G. Fitton, D. L. J. Quicke, Zool. Scr. 1998, 27, 319; b) J. Le Lannic, J. P. Nénon, Zoomorphology 1999, 119, 73; c) C. A. Boring, M. Sharkey, J. Nychka, J. Hym. Res. 2009, 18, 1; d) T. B. H. Schroeder, J. Houghtaling, B. D. Wilts, M. Mayer, Adv. Mater. 2018, 30, 1705322.
- [9] a) K. G. Kornev, A. A. Salamatin, P. H. Adler, C. E. Beard, *Sci. Rep.* 2017, 7, 6582; b) H. W. Krenn, N. P. Kristensen, *Zool. Anz.* 2000, 239, 179; c) G. S. Graham-Smith, *J. Hyg.* 1911, 11, 390.
- [10] a) M. S. Lehnert, D. Monaenkova, T. Andrukh, C. E. Beard,
  P. H. Adler, K. G. Kornev, J. R. Soc., Interface 2013, 10, 20130336;
  b) C. Zhang, P. H. Adler, D. Monaenkova, T. Andrukh, S. Pometto,
  C. E. Beard, K. G. Kornev, J. R. Soc., Interface 2018, 15, 20180229.
- [11] C. Zhang, K. G. Kornev, Surf. Innovations 2017, 5, 194.
- [12] a) W. P. Wall, E. H. Barman, C. M. Beals, Aquat. Insects 2006, 28, 277; b) S. Kehl, in Ecology, Systematics, and the Natural History of Predaceous Diving Beetles (Coleoptera: Dytiscidae) (Ed: D. A. Yee), Springer, London, 2014.
- [13] M. C. Michat, Y. Alarie, K. B. Miller, Syst. Entomol. 2017, 42, 734.
- [14] J. S. Miller, Bull. Am. Mus. Nat. Hist. 1991, 204, 1.
- [15] S. R. Smedley, T. Eisner, Science 1995, 270, 1816.
- [16] C. Zhang, C. E. Beard, P. H. Adler, K. G. Kornev, R. Soc. Open Sci. 2018, 5, 171241.
- [17] C. A. Driscoll, M. A. Condon, Ann. Entomol. Soc. Am. 1994, 87, 448.
- [18] P. A. Coronado-Gonzalez, S. Vijaysegaran, A. S. Robinson, J. Insect Sci. 2008, 8, 11.
- [19] M. I. Crichton, Proc. of the 7th Int. Symp. on Trichoptera, Backhuys Publishers, Leiden, The Netherlands 1992.
- [20] a) D. Monaenkova, M. S. Lehnert, T. Andrukh, C. E. Beard, B. Rubin, A. Tokarev, W. K. Lee, P. H. Adler, K. G. Kornev, J. R. Soc., Interface 2012, 9, 720; b) F. Karolyi, N. U. Szucsich, J. F. Colville, H. W. Krenn, Biol. J. Linn. Soc. 2012, 107, 414; c) J. Guadarrama-Cetina, Eur. Phys. J. E: Soft Matter Biol. Phys. 2014, 37, 6.